JOURNAL OF GEOPHYSICAL RESEARCH, VOL. 111, A09206, doi:10.1029/2005JA011472, 2006

Fast Auroral Snapshot observations of perpendicular DC electric field structures in downward current regions: Implications

K.-J. Hwang,[1] K. A. Lynch,[1] C. W. Carlson,[2] J. W. Bonnell,[2] and W. J. Peria[3]

Received 12 October 2005; revised 13 April 2006; accepted 27 April 2006; published 15 September 2006.

[1] FAST electric field data and ion drift moments are combined to allow full DC $\mathbf{E}_\perp$ (electric field perpendicular to the geomagnetic field) studies of auroral return current regions. Statistical comparison of 71 return current potential structures showed several differences between sheetlike structured perpendicular $\mathbf{E}_\perp$ field events, where the ratio of the two $\mathbf{E}_\perp$ components remains constant during the spacecraft crossing, and curved structures where the ratio varies. Sheetlike structures can be interpreted as straight arcs, but curved structures require gradients in another dimension. We define a parameter η, which is a proxy for the ratio of the potential at the spacecraft and the upgoing electron characteristic energy. Thus η is a measure of the extent to which the potential contours are closed below the spacecraft. Statistical comparison shows that U-shaped closed-potential models are mostly consistent with curved events and ionospheric effects are dominant in sheetlike structures. This result implies that the spatial structure of the events, as indicated by the ratio of the $\mathbf{E}_\perp$ components, allows us to distinguish ionospheric fields and U-shaped potentials. Statistical studies of scale sizes, magnitudes of electric fields and magnetic perturbations, and downward current density, sorted by the parameter η, reveal various interesting features. We attempt to explain these properties on the basis of different potential closure models for sheetlike and curved structures, which have important implications for models of the formation and evolution of potential structures for downward current regions.

Citation: Hwang, K.-J., K. A. Lynch, C. W. Carlson, J. W. Bonnell, and W. J. Peria (2006), Fast Auroral Snapshot observations of perpendicular DC electric field structures in downward current regions: Implications, *J. Geophys. Res.*, *111*, A09206, doi:10.1029/2005JA011472.

1. Introduction

[2] The Freja satellite, launched in 1992, observed extremely intense (of the order of 1 V/m, up to 2 V/m) and fine-structured (a few kilometers) diverging perpendicular electric field events corresponding to positive potential structures at altitudes of 1400 to 1770 km. [*Karlsson and Marklund*, 1996]. The majority of these intense field events are thought to be associated with east-west aligned dark striations rather than black auroral curls. They are related to intense transverse ion fluxes and minimum solar EUV radiation conditions which correspond to low ambient ionospheric conductivity. From these observations, a picture was developed of low-altitude potential structures associated with black aurora and downward or diverging electric fields as the counterpart to negative potential structures in upward current regions [*Marklund et al.*, 1997] (see Figure 1).

[3] Recent simulations [*Streltsov and Marklund*, 2006] of diverging $\mathbf{E}_\perp$ (the electric field perpendicular to the geomagnetic field, $\mathbf{B_0}$) in downward current regions were compared to a case study event from Cluster [*Marklund et al.*, 2001]. These simulations showed that the divergent $\mathbf{E}_\perp$ observed by Cluster can be developed as a result of the interaction between downward field-aligned currents and the ionosphere.

[4] In their previous studies [*Streltsov and Lotko*, 2003a, 2003b], a two fluid MHD simulation showed that intense electric fields and currents can be generated as a consequence of the interaction of a large-scale, slowly evolving current system with a weakly conducting ionosphere.

[5] These numerical studies were based on analytic approaches [*Lysak and Song*, 2002] which showed that the ionospheric feedback instability resulting from the over-reflection of Alfvén waves gives rise to a mechanism for the development of small-scale current structures in the auroral ionosphere.

[6] All these studies imply that ionospheric effects are important for the evolution of structures of $\mathbf{E}_\perp$ at satellite altitudes, suggesting revision of the classical picture of

[1]Department of Physics and Astronomy, Dartmouth College, Hanover, New Hampshire, USA.
[2]Space Sciences Laboratory, University of California, Berkeley, California, USA.
[3]Department of Geophysics, University of Washington, Seattle, Washington, USA.

0148-0227/06/2005JA011472$09.00

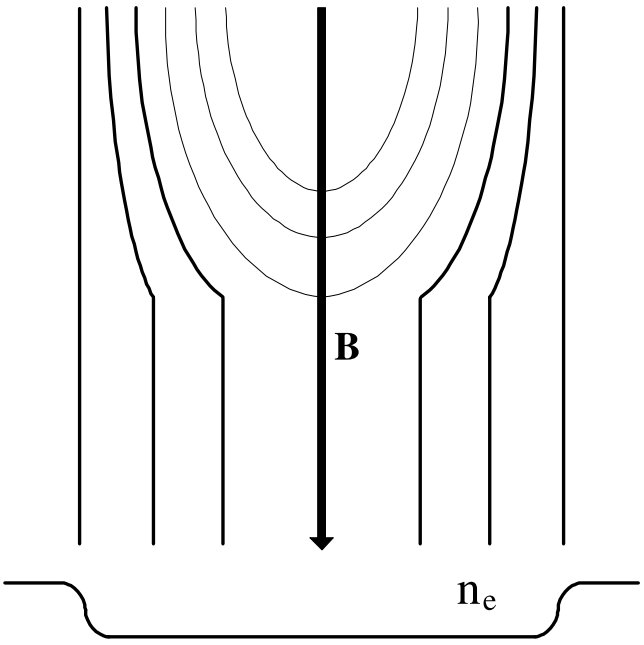

Figure 1. Contours of a composite of U-shaped potentials (thin lines) and ionospheric potentials (thick lines), adapted from *Marklund et al.* [1997].

quasi-static U-shaped potential structures in the downward current region. This has already been suggested by *Marklund et al.* [1997, Figure 1], but a quantitative description of the formation or the underlying mechanism has not yet been presented.

[7] The framework we will use for the observations presented in this paper assumes that both U-shaped and ionospheric potentials contribute to $\mathbf{E}_\perp$ signatures at FAST altitudes. The justification for this picture, based on *Streltsov and Marklund* [2006], presumes a series of physical processes. Magnetospherically required downward field-aligned currents deplete the ionospheric density by encouraging thermal electrons to evacuate from the lower ionosphere, resulting in a localized decrease of Pedersen conductivity. This ionospheric conductivity drop requires large ionospheric perpendicular fields to develop for current continuity and quasi-neutrality reasons, and these $\mathbf{E}_\perp$ propagate upward along the field lines [*Streltsov and Marklund*, 2006]. These apparently overreflected waves associated with evacuating fluxes in the lower ionosphere modify the electrodynamics of upper auroral acceleration regions by the feedback instability [*Lysak and Song*, 2002]. On these evacuated field lines, which are still carrying the externally required downward currents, U-shaped potentials can be expected to form since the situation becomes charge-carrier limited.

[8] A full model of these processes must account for a number of velocities, including the Alfvén transit velocity, the ion acoustic velocity of the escaping thermal flux [*Doe et al.*, 1993], the flow velocity of the ionospheric boundary, and proper motions of the arc structures. Interpretation of observational signatures in these regions must consider both ionospheric and higher altitude processes, as illustrated in Figure 1.

[9] The overview of this paper is as follows. A companion paper [*Hwang et al.*, 2006] introduces the data set of different $\mathbf{E}_\perp$ structures, i.e., the statistics of sheetlike and curved events. In sheetlike events the ratio of the two E field components remains constant during the spacecraft crossing, and in curved structures the ratio varies. The distinction between sheetlike and curved structure is important in that curved structures require gradients in another dimension. In the companion paper we showed that curved structures, rather than sheetlike, predominate in return current regions. This second paper is motivated by the question of what determines sheetlike versus curved structuring. In this paper we show that the significance of ionospheric electric fields is related to the spatial structure. A majority of the events in the study show a disagreement between electron characteristic energies measured from upgoing beams of electrons and potentials measured along the FAST track. This disagreement implies incomplete closure of potentials below the spacecraft as illustrated in Figure 1. Here we explore statistically the implications of this interpretation. A new model combining a superposition of ionospheric fields and U-shaped potentials for downward potential structures is required to explain these FAST observations and is necessary for the development of models of current-voltage relations in the downward current region.

[10] The statistical analysis is based on 71 strong field events from 50 FAST orbit passes mostly comprised of higher time-resolution burst data. We also present typical examples for each of several different $\mathbf{E}_\perp$ structure types.

2. Data Examples

2.1. Short Summary of Companion Paper Concerning Structural Signatures and Preliminary Statistics

[11] Using the methods described by *Hwang et al.* [2006] to extract both spin-plane and spin-axis components of perpendicular DC electric field, we classify 71 FAST downward current region intense electric field (>100 mV/m) events into three categories: sheetlike, corresponding to a straight sheetlike arc; curved, corresponding to filaments or curved structures such as curls, folds, or vortices; and changing, where structural properties vary across the event. We define sheetlike events as those for which $\mathbf{E}_{\mathbf{east}}/\mathbf{E}_{\mathbf{north}}$ remains constant during the spacecraft crossing and curved as those where this ratio varies. Sheetlike structures can be interpreted as straight arcs, but curved structures require gradients in another dimension.

[12] In the companion paper, scatterplots of the scale length of $\mathbf{E}_\perp$ versus the scale length of current sheet and of the magnitude of $\mathbf{E}_\perp$ versus the scale length of $\mathbf{E}_\perp$ showed that neither scale size nor magnitude of field could distinguish clearly between sheetlike and curved events. In this paper we show that this distinction is well sorted by whether the potentials appear to close below the spacecraft or are coupled to the ionosphere.

2.2. Case Studies: Spatial Structure and Potential Closure

[13] FAST **E** field measurements can be used as a signature of potential structures through which the spacecraft crosses. The potential contours across an auroral arc can be obtained by integrating $\mathbf{E}_\perp$ along the spacecraft

trajectory. The electric field component which contributes to this integrated potential is only the spin-plane (along-track) component ($\mathbf{E_{av}}$), since the spin-axis (along-arc) component from ion drift moments in the ram spacecraft velocity direction is normal to the payload velocity.

[14] Assuming that the equipotential surfaces crossed by FAST are closed below the payload, this potential structure can also be measured from the characteristic energies of upgoing ionospheric electrons ($\epsilon_{\mathbf{ce}}$) accelerated by parallel potential drops [*Carlson et al.*, 1998]. Perfect agreement between these field and particle potential signatures implies a complete closure of the potential contours between the satellite and the source of the upgoing electrons. A disagreement between them implies that the closure of the potentials is not complete and that some of the potential structure couples to the lower ionosphere.

[15] To measure this closure, we can compare the electron characteristic energies to the potentials calculated by integrating electric field along the FAST trajectory ($-\int \mathbf{E_{av}} \cdot \mathbf{ds}$) as just described above. Equivalently, we can compare the derivative of the electron characteristic energies along the trajectory ($\delta\epsilon_{\mathbf{ce}}$) to the electric field measurements along the spacecraft ($\mathbf{E_{av}}$) as shown in Figure 2e. The latter is preferred in order to avoid an arbitrary offset problem in calculating integrated potentials. The electric field instrument measurements (30 μs) have been filtered to the same sampling time as the electron-spectra-derived measurements (78 ms).

[16] Figure 2a shows a sheetlike example (FAST orbit 1750), Figure 2b shows a curved example (FAST orbit 5453), and Figure 2c shows a changing example (FAST orbit 1753). In the bottom panel of each, the green profile corresponds to the electric field measurement along the trajectory ($\mathbf{E_{av}}$) and the black to the derivative of the electron characteristic energy ($\delta\epsilon_{\mathbf{ce}}$).

[17] For the sheetlike case, the peak value of $\mathbf{E_{av}}$ is much larger than that of $\delta\epsilon_{\mathbf{ce}}$ during the strong field event. For the curved example the peak values of $\mathbf{E_{av}}$ and $\delta\epsilon_{\mathbf{ce}}$ are quite similar. For the changing example, we find the peak of $\mathbf{E_{av}}$ larger than that of $\delta\epsilon_{\mathbf{ce}}$ during the sheetlike portion of the event and matching during the curved portion.

[18] The implication drawn from this different closure between sheetlike and curved examples is that the two perpendicular spatial structure types (sheetlike and curved) have different altitudinal structures for their potentials as well. For the sheetlike events the potentials at least partially couple to the ionosphere, while for the curved events, complete closure of U-shaped potentials is seen. In the next section we show that the trend of these case studies is confirmed with statistics.

3. Statistical Analysis

[19] We now expand these case studies to a statistical study. The database of 71 events contains observations from downward current region crossings between 2500 km and 4100 km altitude, from either the prenoon dayside or near midnight. For each event, the following parameters are recorded: sheetlike or curved, the scale length of the downward current sheet ($\mathbf{L_{\delta B}}$), the scale length of $\mathbf{E}_\perp$ ($\mathbf{L_{E_\perp}}$), peak $\mathbf{E}_\perp$, $\mathbf{j}_\parallel$ as defined by $\mathbf{\delta B/L_{\delta B}}$, and η as defined below. The scale length $\mathbf{L_{\delta B}}$ is taken as the overall extent of the positive slope region of $\mathbf{\delta B}$ (this is sometimes clearer in longer time plots than are shown here). The scale length $\mathbf{L_{E_\perp}}$ is meant to be the extent of the electric field event; that is, we look for boundaries where the coherent event signatures deviate from the background nonevent level. This is a somewhat subjective description but we use the result for only fairly qualitative comparisons. The sheetlike or curved designation is given as a qualitative parameter running from purely sheetlike (0.0) to fully curved (1.0) with three midlevels.

3.1. Parameter $\delta\epsilon_{ce}/\mathbf{E_{av}}$, η

[20] The ratio

$$\eta = \delta\,\epsilon_{ce\,\mathbf{pp}}/\mathbf{E_{av\,pp}}$$

is chosen as a useful parameter for comparing particle and field profiles of the potential structure. For each event the value of η is calculated from peak-to-peak magnitudes of $\mathbf{E_{av}}$ and $\delta\epsilon_{\mathbf{ce}}$ within each $\mathbf{E}_\perp$ event. The statistics below confirm the relationships shown in the case studies: curved events have η near 1, implying potential closure between the spacecraft and the source of upgoing electrons; sheetlike events have $\eta < 1$, implying incomplete closure and ionospheric electric fields.

[21] Figure 3 shows the statistics of the relationship between the degree of sheetlike or curved behavior, and η, where 0 in the y-axis indicates purely sheetlike events and 1 indicates purely curved. For consistency with subsequent plots, sheetlike events are shown in red, curved in green, and changing in blue. Events for which $\eta > 1$ (13 out of 71) do not fit our model and are not considered here: a larger field-aligned than perpendicular potential difference cannot be pictured by either U-shaped potentials or ionospheric fields. These events must be explained with a more complicated model such as time variation during the crossing. Considering only $\eta \leq 1$ events, we see that most sheetlike events have η below 0.4, and most curved events have η above 0.6. Thus unlike scale sizes or field or current magnitudes, the parameter η and its implication for potential closure below the observation point sorts clearly between sheetlike and curved perpendicular events.

[22] The classical U-shaped equipotential model still works well for curved events where $\eta \approx 1$. If sheetlike events are not consistent with potential closure below the observation point, then ionospheric fields must be considered, as depicted by the thick lines in Figure 1 and as expected from theoretical *Lysak and Song* [2002] and numerical *Streltsov and Lotko* [2004] studies.

3.2. Discussion: Overlap of Ionospheric Fields and U-Shaped Potentials for Sheetlike and Curved Events

[23] The generation of ionospheric fields has been studied both analytically and computationally in the context of feedback instabilities for small scale size regions. Here we build on these studies [*Lysak and Song*, 2002; *Streltsov and Lotko*, 2003a, 2003b, 2004; *Streltsov and Marklund*, 2006] to interpret our observations as composite potential structures consisting of both U-shaped potentials and ionospheric fields.

[24] An externally required downward field-aligned current induces ionospheric electrons to move upward along

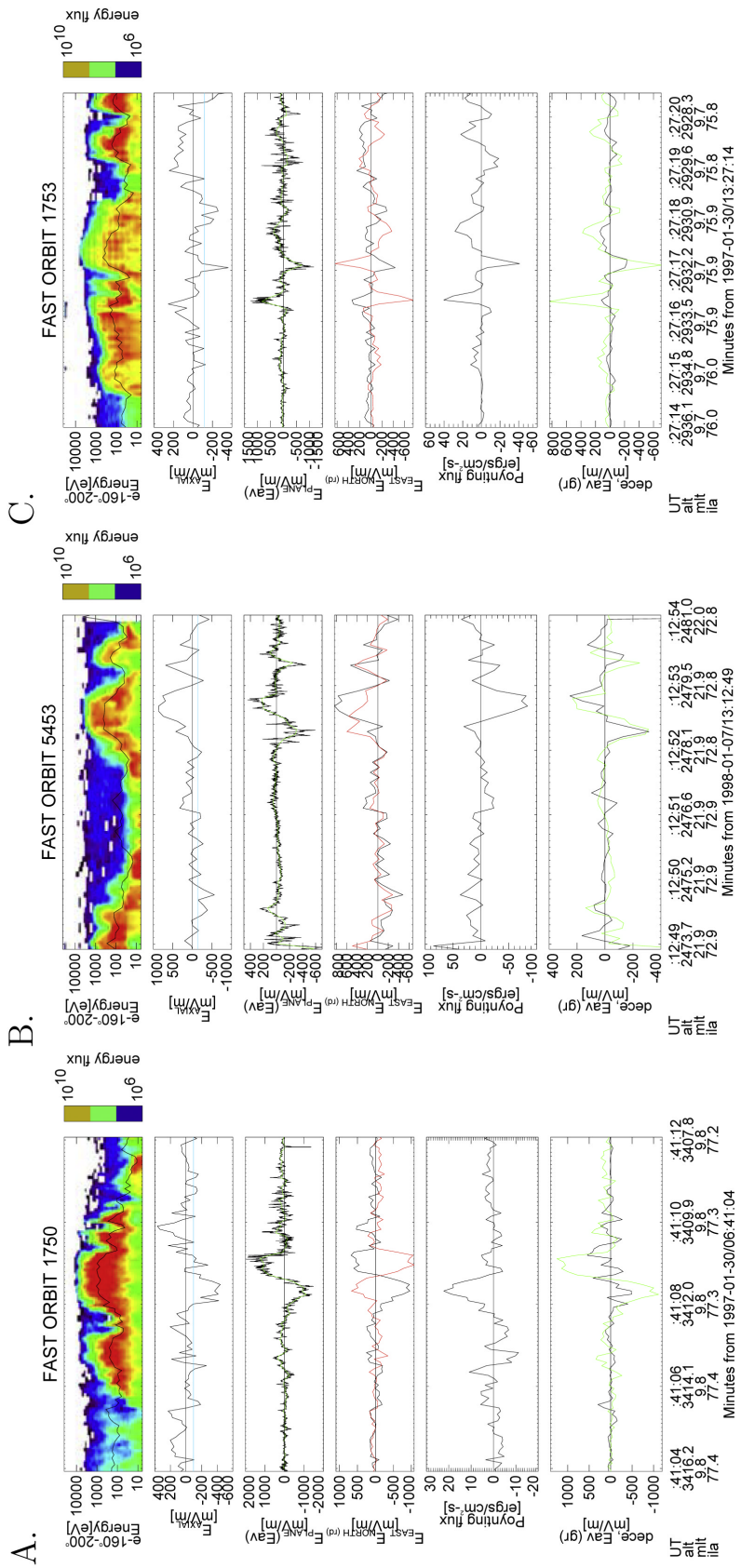

Figure 2. Case studies: (1) sheetlike example, orbit 1750, (2) curved example, orbit 5453, (3) changing example, orbit 1753. (a) Upgoing electron energy spectrogram, (b) the spin-axial component of $\mathbf{E}_\perp$ calculated from ion distributions, (c) the spin-plane component of $\mathbf{E}_\perp$ "E-along-velocity" observed by FAST field measurements, (d) two $\mathbf{E}_\perp$ components transferred to the geographic coordinates (black: east-west, red: north-south components), (e) Poynting flux measured from $\mathbf{E}_\perp \times \delta\mathbf{B}$, (f) the derivative of upgoing electron characteristic energy ($\delta\epsilon_{ce}$, black) with $\mathbf{E}_{av}$ measured along FAST trajectory (green).

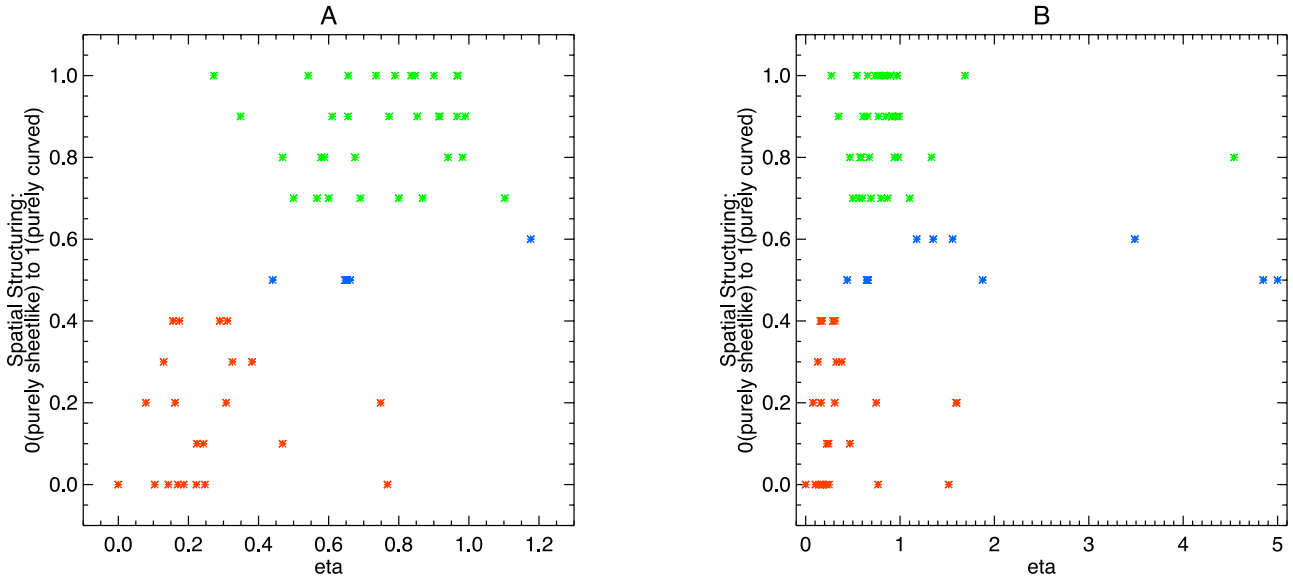

Figure 3. Dependence of spatial structuring—sheetlike or curved as evidenced by nature of $\mathbf{E_{north}/E_{east}}$—on closure and coupling of potentials below the observation point as parameterized by η (a measure of potential closure as described in the text). For consistency with later plots, sheetlike examples are shown in red, curved in green, and changing in blue. One point is shown for each of the 71 examples. (a) Events with $\eta \leq 1.2$; (b) all values of η.

the magnetic field lines. As a result, it evacuates electrons from the ionosphere along the magnetic field and reduces the Pedersen conductivity at the footpoint in the lower ionosphere. A localized decrease of Pedersen conductivity requires a large perpendicular electric field for current continuity and quasi-neutrality reasons in the ionosphere. The large perpendicular electric field pushes ions horizontally away from the center of the current channel [*Streltsov and Marklund*, 2006]. This ionospheric electric field couples along the field line, fading with altitude as the field lines diverge. Electrons are moved along the magnetic field maintaining current balance and a quasi-neutrality requirement. Eventually, the field line becomes charge-carrier limited just as in inverted-V cases, and U-shaped field-aligned potential differences form to maintain the electron current densities while maintaining neutrality. Given this scenario, the formation of U-shaped potentials on return current field lines is tightly tied to the formation and evolution of the ionospheric response. At FAST altitudes, both signatures are apparent.

[25] In Figure 3 we see that for most sheetlike cases, the potential structures contains significant ionospheric field effects as well as classic U-shaped potentials. Curved structures are better modelled by the U-shaped equipotential model.

[26] This picture is consistent with Poynting flux observations. The three examples of Figure 2 show Poynting flux in Figure 2e. For sheetlike structures (Figure 2a), upward Poynting flux is dominant, while curved structures (Figure 2b) tend to be accompanied by downward Poynting flux. Figure 4 shows the statistics of Poynting flux as a function of η. Again colors are coded as red for sheetlike, green for curved, and blue for changing events. Positive Poynting flux corresponds to upward propagation and negative to downward. For the events of $\eta \leq 0.4$, the upward propagations dominate (15 events out of 21), and for the events of $\eta \geq 0.6$, the downward propagations dominate (18 events out of 25). The earlier part of the temporal evolution of the structure, that is, the coupling of ionospheric fields from the lower ionospheric conductivity (density) hole may look the same as an overreflection of downgoing Alfven waves. Still, the Poynting flux statistics are consistent with the picture of the temporal evolution of combined ionospheric fields and U-shaped potential structures: sheetlike events, caused by ionospheric fields, show upgoing Poynting fluxes from a lower altitude source, and curved events, driven by higher altitude potentials, show downgoing Poynting fluxes.

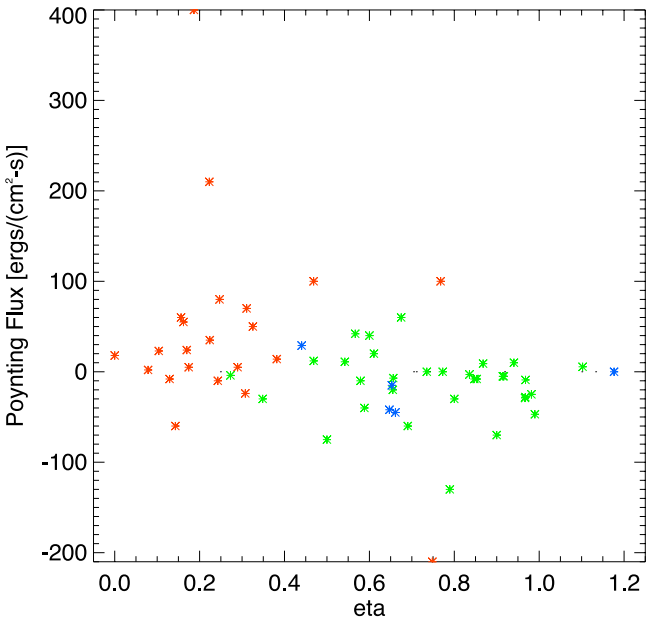

Figure 4. Poynting flux as a function of η.

[27] These composite potential structures suggest a new approach to determining current-voltage relations in downward current regions. Clearly, only the U-shaped part of the potential structures should be considered. We might expect a current-voltage region similar to the upward current Knight relations for curved potential structures since these are dominated by U-shaped potentials. The observed time period of the formation and growth of the potential structure of the downward current region is observed to be comparable to the time needed to evacuate ionospheric electrons over the downward current region [*Marklund et al.*, 2001]. Since the formation of the potential drop of U-shaped potentials is triggered by the charge limitation due to the evacuation of the ionospheric density by the downward current, the parallel potential drop in downward current regions is presumably related to the charge limitation of ionospheric particles rather than by the mirroring effect of magnetospheric particles. However, statistical scatterplots of integrated potential drops versus downward current densities for the curved events do not show a strong correlation. This expected correlation may be masked by the fact that the spacecraft, at FAST altitudes, does not always traverse the full potential drop.

[28] Figure 3 tells us that a distinguishing, perhaps causal, feature between curved and sheetlike events is the degree to which the potential structures close or couple to the ionospheric boundary. Next we examine statistically the dependence of this closure or coupling, as quantified by η, on other parameters such as current density, scale size, or field magnitudes.

4. Parameterization

[29] We have begun our discussion with a proposed series of physical processes associated with the formation of ionospheric fields and how they are overlapped with U-shaped potentials. Next we consider statistical studies of scale sizes, magnitudes of electric fields and magnetic perturbations, and downward current density, as sorted by the parameter η, revealing various interesting features. We attempt to explain these features on the basis of different potential models for sheetlike and curved structures, considering both altitudinal and perpendicular structure of the potentials.

[30] Figure 5 shows the statistical relationships between η and $\mathbf{j}_{\parallel}$ (Figure 5a), the scale size of $\mathbf{\delta B}$ (the magnetic fluctuation perpendicular to the geomagnetic field, $\mathbf{B_0}$) (Figure 5b), the peak magnitude of $\mathbf{E}_{\perp}$ (Figure 5c), and the spatial gradient of $\mathbf{E}_{\perp}$ (Figure 5d). Again the coloring of the points indicates sheetlike (red), curved (green), or changing (blue) events. For these plots only events with $\eta \leq 1$ are considered.

4.1. Parameter $\mathbf{j}_{\parallel}(\eta)$ (Figure 5a)

[31] We consider first $\mathbf{j}_{\parallel}(\eta)$ as shown in Figure 5a. The spatial structure (sheetlike, curved, or changing) is well-sorted along the **x**-axis, i.e., according to the value of η. The dependence of $\mathbf{j}_{\parallel}$ on η is not as obvious and depends also on the spatial structure as indicated by color.

[32] It is interesting to consider the plot divided into four quadrants, (large/small η, large/small $\mathbf{j}_{\parallel}$). In quadrant 1 where both are large, all events are curved cases. In quadrant 3 where both are small, all are sheetlike. In the two quadrants 2 and 4, both sheetlike and curved events are seen.

4.2. Parameter $\mathbf{L_{\delta B}}(\eta)$ (Figure 5b)

[33] Figure 5b plots the scale length of the current sheet for each event as a function of η. Events with significant ionospheric signatures (small η, sheetlike events) are confined to a smaller range of current sheet scales than U-shaped (curved) events. Small η events (mostly sheetlike) are found for $\mathbf{L_{\delta B}}$ below about 150 km; larger η events (mostly curved) are seen with current sheets up to twice as wide. For curved events there is a weak positive correlation between $\mathbf{L_{\delta B}}$ and η: events more completely closed off from ionospheric fields tend to be embedded in larger scale current sheets.

4.3. Parameter $\mathbf{E}_{\perp}(\eta)$ (Figure 5c)

[34] Figure 5c shows the magnitude of $\mathbf{E}_{\perp}$ as a function of η. Small η (sheetlike) events cover a larger range of $\mathbf{E}_{\perp}$ values, and large η events are confined to $\mathbf{E}_{\perp}$ below 500–600 mV/m. This is consistent with the scale size arguments of the previous figure as the potential gradients are confined to small perpendicular scales for small η. It is inconsistent, though, with models of curls from $\mathbf{E} \times \mathbf{B}$ instabilities, for which stronger $\mathbf{E}_{\perp}$ would indicate stronger curvature. For sheetlike events, there is a weak positive correlation between $\mathbf{E}_{\perp}$ and η.

4.4. Parameter $\mathbf{E}_{\perp}/\mathbf{L}_{\mathbf{E}_{\perp}}(\eta)$ (Figure 5d)

[35] We combine the magnitude of $\mathbf{E}_{\perp}$ with its scale size $\mathbf{L}_{\mathbf{E}_{\perp}}$ within a current sheet in Figure 5d, showing $\mathbf{E}_{\perp}/\mathbf{L}_{\mathbf{E}_{\perp}}$ as a function of η; here we consider the gradients and shears in the electric fields as a function of closure/coupling to the ionosphere. Now, both sheetlike and curved examples show positive correlations with η, but with different proportionalities.

[36] In either case, as $\mathbf{E}_{\perp}$ increases or $\mathbf{L}_{\mathbf{E}_{\perp}}$ decreases, the degree of closure from the ionospheric boundary increases. However, the two groups (sheetlike and curved) behave with different trends and do not merge into each other with increasing η.

5. Discussion

[37] The parameterization by η of scale sizes and field magnitudes for these different structures can be considered in light of the magnetic fracture model of auroral potential drops [*Haerendel*, 1989; *Paschmann et al.*, 2002]. The composite potential structures considered here include both ionospheric fields strongly tied to the lower ionosphere, and U-shaped potentials that are decoupled from the lower boundary. Models of the evolution of these structures need to consider flows and proper motions at both ends.

[38] Figure 5c shows that the strongest magnitude events seen are those with both U-shaped potentials and ionospheric contributions ($\eta \approx 0.3$–0.4). In the processes outlined above, the evacuated field line above an ionospheric divergent field develops a U-shaped potential for charge carrier limitation reasons; the U-shaped potential is nested within the ionospheric equipotential contours as shown in Figure 1. Thus for these combined potential events, while the U-shaped potential itself is decoupled from the footpoint

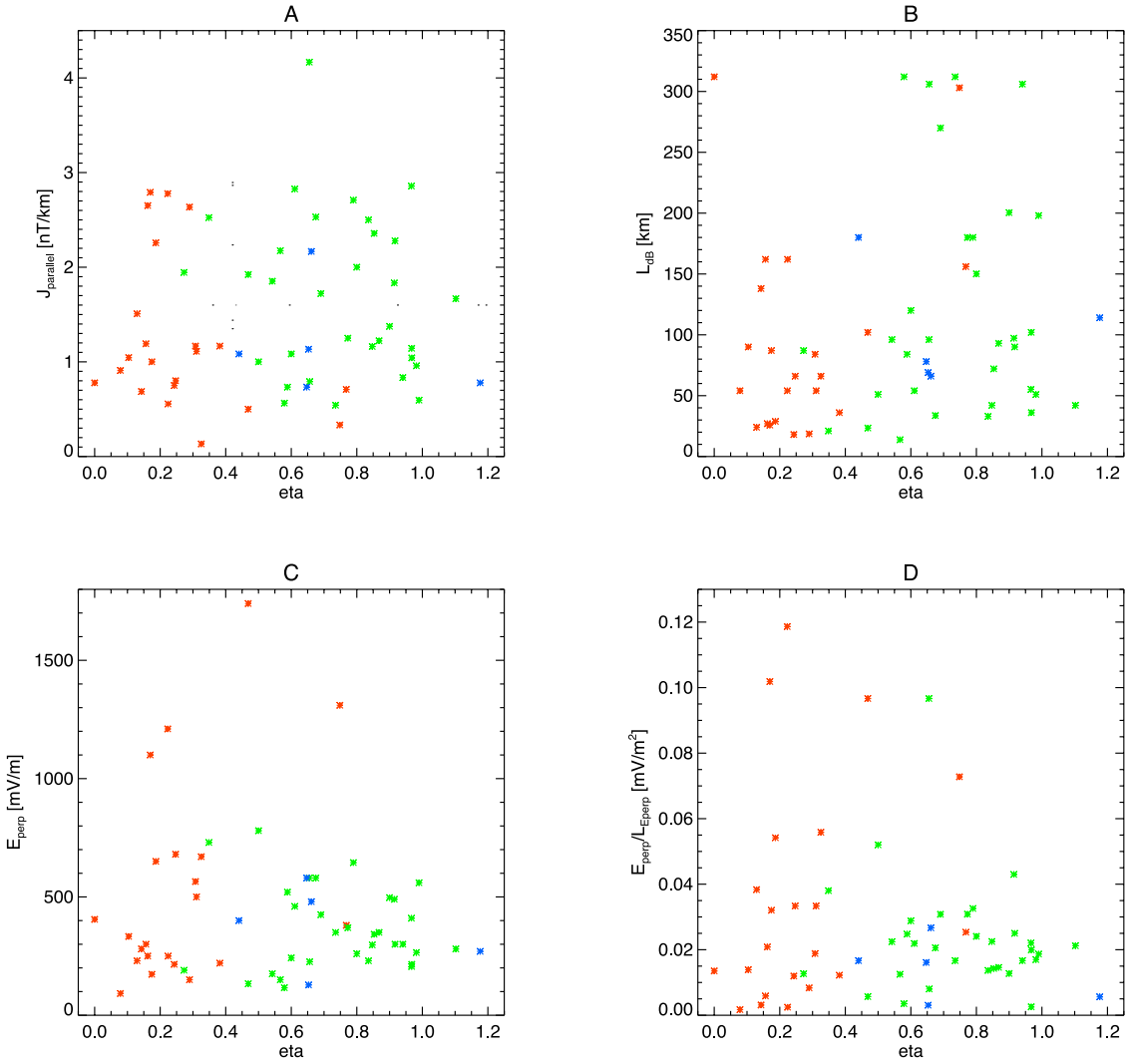

Figure 5. Scatterplots of the η dependence of (a) parallel current density $\mathbf{J}_{\|}$, (b) scale length of the current structure $\mathbf{L}_{\delta\mathbf{B}}$, (c) magnitude of the electric field $\mathbf{E}_{\perp}$, and (d) gradient of electric field $\mathbf{E}_{\perp}/\mathbf{L}_{\mathbf{E}_{\perp}}$. Again, sheetlike examples are shown in red, curved in green, and changing in blue.

and widens to acquire more charge carriers [*Aikio et al.*, 2004], its motion and evolution may be constrained by the exterior, sheetlike, ionospheric field.

[39] Our interpretation is that during the earliest stages of the formation of the composite potential structures, the nested U-shaped potentials are not free enough to form folds and curls according to Kelvin-Helmholtz or tearing mode instabilities because they are confined by the ionospheric conductivity structure. At a later time after the relaxation of the ionospheric field and widening of the current channel [*Marklund et al.*, 2001; *Aikio et al.*, 2004; *Streltsov and Marklund*, 2006], the high-altitude potentials could form folds or filaments which are observed as curved structures by FAST. During this period, the downward current density and the potential drop would be kept as constant. This discussion may be somewhat speculative, given that the time evolution processes are unsubstantiated by the single-point FAST data. One way to confirm the evolutionary scenario might be ground camera observations.

[40] Altitudinal structures of return current potentials are also of interest. Ionospheric fields fall off with altitude as $1/r^{3/2}$ as the field lines diverge [*Mozer*, 1970]. Models of return current region U-shaped potentials predict upward motion of the structures at the ion acoustic velocities [*Ergun*, 2003]. It has also been found that parallel potential drops that are a function of the field-aligned current density are diffusive and tend to smooth out small scales by ionospheric feedback instabilities [*Lysak and Song*, 2002]. Thus the $\mathbf{E}_{\perp}$ of U-shaped potentials can be weakened as they move upward along the magnetic field lines while ionospheric field effects become faint as they fall away with altitude because of the diverging geometry of the magnetic field. Thus the relative strength of the ionospheric field versus U-shaped potential field is a sensitive function of altitude and time evolution.

[41] Charge carrier limitation on evacuated field lines causes the formation of U-shaped potentials, perhaps repeatedly, either intermittently or periodically, eventually giving rise to a series of field-aligned potential drops in a parallel direction, similar to double layers separated along field lines [*Lysak and Dum*, 1983; *Lysak and Hudson*, 1987; *Sato and Okuda*, 1981; *Andersson*, 2002]. If the repeated upward

moving U-shape structures are nested along a single large field line, the spacecraft could see either a single potential structure or a series of S-shaped potential structures as the spacecraft cuts across the nested structures. In the latter case one might expect a stairstep appearance in the perpendicular potential profile. However, whenever we see neighboring strong events, the potential seems to return to a baseline between them. This observation may help constrain models of the altitudinal evolution of these U-shaped structures.

6. Conclusion and Future Work

[42] Following a companion paper, we investigate electric field signatures in downward current regions, focusing on the distinctions between sheetlike and curved potential structures.

[43] 1. We propose a composite potential structure for these signatures, with contributions of varying magnitude from both ionospheric $\mathbf{E}_\perp$ and from U-shaped potentials. For U-shaped potentials, the energy gained by upgoing electrons through the structure is equal to the integrated $\mathbf{E}_\perp$ seen by the payload as it crosses the structure. Events for which the electron energy is less than $\int \mathbf{E_{av}} \cdot \mathbf{ds}$ are interpreted as having incomplete closure from ionospheric fields.

[44] 2. We construct a parameter η to measure this closure, and find that curved events have high η (more closure) and sheetlike events have small η (more ionospheric fields). This interesting relationship connects two totally separate classifications of events: whether $\mathbf{E_{north}}/\mathbf{E_{east}}$ is consistent with sheetlike or curved/filamentary potential structures and whether the potential structures are closed from the ionospheric fields.

[45] 3. Thus it can be concluded that perpendicular electric fields in the downward current region observed at FAST altitudes are caused by both ionospheric effects and by U-shaped potentials, and the structural signature of the electric field allows us to distinguish them.

[46] 4. There is no direct correlation between $\mathbf{j}_\parallel$ and η. Events with small values of both $\mathbf{j}_\parallel$ and η are all sheetlike, and events with large values of both $\mathbf{j}_\parallel$ and η are all curved.

[47] 5. Events with small η (sheetlike, ionospheric) are found in current sheets of smaller scale length; higher η (curved, U-shaped) events cover a larger range of $\mathbf{L_{\delta B}}$.

[48] 6. Events with small η (sheetlike, ionospheric) reach stronger values of $\mathbf{E}_\perp$; higher η (curved, U-shaped) are confined to a small range of $\mathbf{E}_\perp$.

[49] 7. Both sheetlike and curved events show positive correlations between $\mathbf{E}_\perp/\mathbf{L}_{\mathbf{E}_\perp}$ and η, but with different proportionalities.

[50] 8. For curved events presumed to be dominantly U-shaped potentials, a current-voltage relation could be expected for charge limitation reasons. However, statistics of potential versus $\mathbf{j}_\parallel$ do not show a correlation; this may be because FAST passes do not cross the full potential of the flux tube.

[51] In general, we wish to stress that models of current-voltage relations in return current regions need to consider ionospheric effects on charge limitation. Since the electric fields may not close at the bottom of a sheath, and instead can couple to low altitudes, a linear relationship between downward current density and parallel potential drop is not easily conjectured.

[52] Downward field-aligned currents are closely tied to ionospheric fields and changes of Pedersen conductivity or plasma density, so in order to formulate current-voltage relations here, we need analytic models that incorporate ionospheric evolution.

[53] Ultimately, the observational study of the structure of downward current region potential structures using $\mathbf{E}_\perp$ will give models of their formation, generation, and evolution. We hope these data will help constrain and direct these models.

[54] **Acknowledgments.** We thank both reviewers and the editor for their thoughtful and constructive comments. This work was supported by NASA grant NAG5-10472 and by Dartmouth College.

References

Aikio, A. T., K. Mursula, S. Buchert, F. Forme, O. Amm, G. Marklund, M. Dunlop, D. Fontaine, A. Vaivads, and A. Fazakerley (2004), Temporal evolution of two auroral arcs as measured by the cluster satellite and coordinated ground-based instruments, *Ann. Geophys.*, *22*, 4089.

Andersson, L. (2002), Characteristics of parallel electric fields in the downward current region of the aurora, *Phys. Plasmas*, *9*, 3600.

Carlson, C. W., et al. (1998), FAST observations in the downward auroral current region: Energetic upgoing electron beams, parallel potential drops, and ion heating, *Geophys. Res. Lett.*, *25*, 2017.

Doe, R. A., M. Mendillo, J. Vickrey, L. Zanetti, and R. Eastes (1993), Observations of nightside auroral cavities, *J. Geophys. Res.*, *98*, 293.

Ergun, R. (2003), Double layers in the downward current region of the aurora, *Nonlinear Proc. Geophys.*, *10*, 45.

Haerendel, G. (1989), Cosmic linear accelerators, *Eur. Space Agency Spec. Publ.*, *ESA SP-285*.

Hwang, K., K. Lynch, C. Carlson, J. Bonnell, and W. Peria (2006), FAST observations of perpendicular DC electric field structures in downward auroral current regions: Morphology, *J. Geophys. Res.*, doi:10.1029/2005JA011471, in press.

Karlsson, T., and G. T. Marklund (1996), A statistical study of intense low-altitude electric fields observed by Freja, *Geophys. Res. Lett.*, *23*, 1005.

Lysak, R. L., and C. T. Dum (1983), Dynamics of magnetosphere-ionosphere coupling including turbulent transport, *J. Geophys. Res.*, *88*, 365.

Lysak, R. L., and M. K. Hudson (1987), Effect of double layers on magnetosphere-ionosphere coupling, *Laser Particle Beams*, *5*, 351.

Lysak, R. L., and Y. Song (2002), Energetics of ionospheric feedback interaction, *J. Geophys. Res.*, *107*(A8), 1160, doi:10.1029/2001JA000308.

Marklund, G., T. Karlsson, and J. Clemmons (1997), On low altitude particle acceleration and intense electric fields and their relationship to black aurora, *J. Geophys. Res.*, *102*, 17,509.

Marklund, G. T., et al. (2001), Temporal evolution of acceleration structures in the auroral return current region, *Nature*, *414*, 724–727.

Mozer, F. S. (1970), Electric field mapping from the ionosphere to the equatorial plane, *Planet. Space Sci.*, *18*, 259.

Paschmann, G., , S. Haaland, and R. Treumann (Eds.) (2002), Auroral plasma physics, *Space Sci. Rev.*, *103*, 1–485.

Sato, T., and H. Okuda (1981), Numerical similuations on ion acoustic double layers, *J. Geophys. Res.*, *86*, 3357.

Streltsov, A. V., and W. Lotko (2003a), Reflection and absorption of alfvenic power in the low-altitude magnetosphere, *J. Geophys. Res.*, *108*(A4), 8016, doi:10.1029/2002JA009425.

Streltsov, A. V., and W. Lotko (2003b), Small-scale electric fields in downward current channels, *J. Geophys. Res.*, *108*(A7), 1289, doi:10.1029/2002JA009806.

Streltsov, A. V., and W. Lotko (2004), Multiscale electrodynamics of the ionosphere-magnetosphere system, *J. Geophys. Res.*, *109*, A09214, doi:10.1029/2004JA010457.

Streltsov, A. V., and G. T. Marklund (2006), Divergent electric fields in the downward current channels, *J. Geophys. Res.*, doi:10.1029/2005JA011196, in press.

J. W. Bonnell and C. W. Carlson, Space Sciences Laboratory, University of California, Berkeley, CA 94720, USA. (jbonnell@ssl.berkeley.edu; cwc@ssl.berkeley.edu)

K.-J. Hwang and K. A. Lynch, Department of Physics and Astronomy, Dartmouth College, 6127 Wilder Laboratory, Hanover, NH 03755, USA. (kyoung-joo.hwang@dartmouth.edu; kristina.lynch@dartmouth.edu)

W. J. Peria, Department of Geophysics, University of Washington, Box 351310, Seattle, WA 98195, USA. (peria@ess.washington.edu)